Gulf of Mexico Science

Volume 22
Number 1 *Number 1*

Article 3

2004

Slope and Roughness Statistics of the Northern Gulf of Mexico Seafloor With Some Oceanographic Implications

Alexis Lugo-Fernández
Office of Leasing and Environment

Michelle M. Morin
Office of Leasing and Environment

DOI: 10.18785/goms.2201.03

Gulf of Mexico Science, 2004(1), pp. 22–44

Slope and Roughness Statistics of the Northern Gulf of Mexico Seafloor With Some Oceanographic Implications

ALEXIS LUGO-FERNÁNDEZ AND MICHELLE M. MORIN

We analyzed 11 cross-slope and six along-slope bathymetric profiles over the continental slope of the northern Gulf of Mexico using statistical and time series techniques. Linear regressions account for over 93% of the water depth variability in nine north–south profiles; the remaining profiles follow quadratic polynomials accounting for over 92% of the variability. Seafloor gradients from the linear fits are generally ≤1°, but local gradients can reach ≅16° near the Sigsbee Escarpment (SE), which is smaller than previously documented. Seafloor roughness elements reach 13–300 m, with most <100 m. Such rough bottoms could affect waves with wavelengths of tens of kilometers but not waves of hundreds of kilometers. Water depth power spectra are red (having the most energy at scales ≥10 km) and exhibit a k^{-2} dependence. Power spectra of short-scale gradients are near constant at scales >0.02 cpkm, implying a white noise process, and overall, these spectra exhibit an exponential dependence. Oceanographically, the slopes are large enough for topographic β-effects to dominate over the planetary β-effect, which allows approximating the topographic Rossby waves (TRWs) dispersion in terms of the Brunt–Vaisala frequency and bottom gradients. The steep SE can sustain minimum periods of ~18 d, which agrees with observed periods. Bottom trapping caused by stratification should be effective only for short waves, but observations suggest that bottom trapping is independent of wavelength. This discrepancy can be explained by the fact that the Gulf of Mexico can be approximated as a two-layer ocean, and TRWs are bottom trapped regardless of wavelength. The critical frequency and slope show that only diurnal and inertial frequencies (at this latitude) could be inducing strong vertical mixing on the study area. The initial conjecture that cyclonic eddies with diameters of 40–150 km are generated by flow-topography interaction was not upheld because the resonance conditions are not met. Finally, the analysis reveals that fluids inside basins cannot escape.

As containers, oceanic basins affect and constrain sea circulation (Sverdrup et al., 1942; Kennett, 1982; Holloway and Merrifield, 1999). The basin's dimensions and the seafloor gradients determine horizontal and vertical modes of the circulation, e.g., Gill (1982). Seafloor topography and roughness produce energy dissipation and mixing, which affect circulation at all scales (Bell, 1975; Rhines, 1977; Hogg, 1995; Munk, 1997). In addition, information on seafloor gradients help understand geological processes acting in a region and their effects on marine acoustics through sound scattering (Fox and Hayes, 1985; Adams and Schlager, 2000). Thus, knowledge of seafloor gradients and roughness is relevant to many areas of scientific research. In this study, we examine seafloor gradients and roughness of the northern Gulf of Mexico. A motivation for this research was our conjecture that topography and eddies had similar scales (40–150 km) over the Gulf's northern continental slope. Furthermore, we attempt to explain the seafloor gradient distribution using current knowledge of regional geology and sedimentation processes. We ascertain the influence of gradients on the regional circulation and how they affect the characteristics and propagation of topographic Rossby waves (TRWs) in the Gulf.

Geologically, the continental slope of the northern Gulf of Mexico, Figure 1, is well known and understood as shown by the recent reviews of Roberts et al. (1999) and Bryant and Liu (2000). This physiographic province is divided into the Louisiana–Texas slope (LTS) and the Mississippi–Alabama slope (MAS). The area encompasses three major features: the Mississippi Canyon (MC), the Mississippi Fan, and the Sigsbee Escarpment (SE). The MC is the divide between the LTS and MAS. The LTS is in turn subdivided into an upper and lower slope (Amery, 1978). The northern continental slope is the widest (230 km) of the Gulf, and its seafloor is very rugged (Bryant and Liu, 2000). The roughness results from the interplay of salt tectonics, sedimentation, and diapirism (Roberts et al., 1999). Many domes and

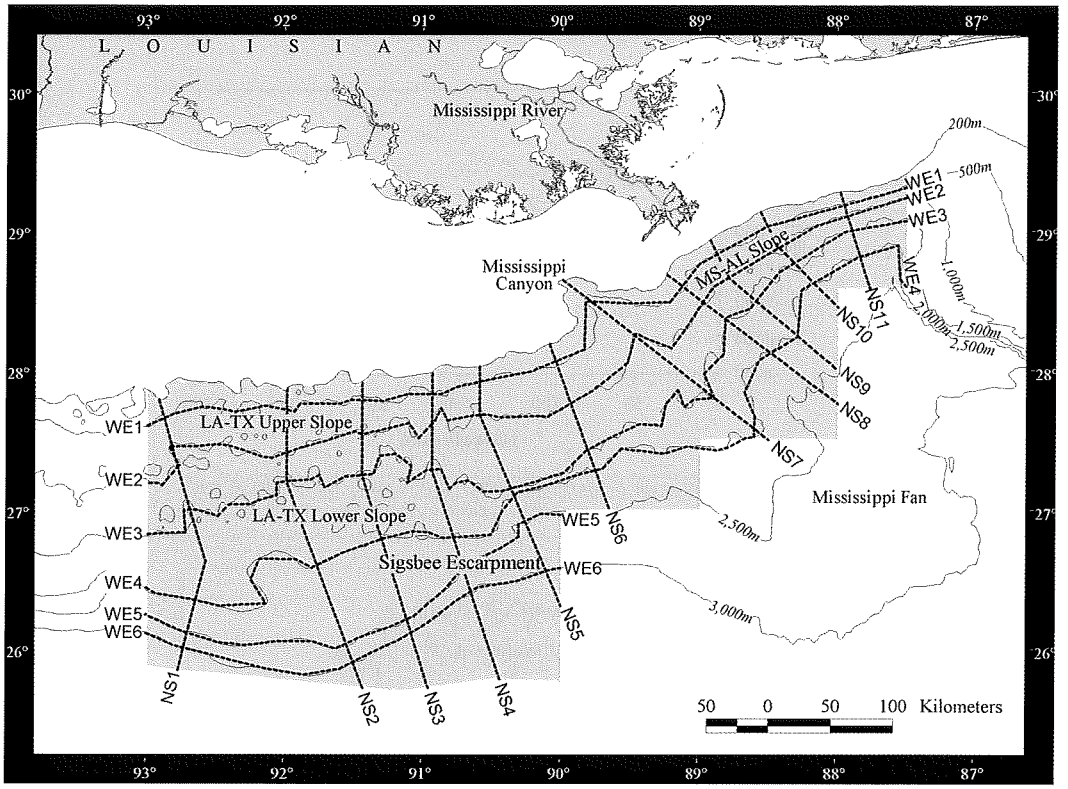

Fig. 1. Layout of the 11 cross-slope (NS lines) and six along-slope (WE lines) profiles (dashed lines) used in this study. Profiles cut across the Louisiana–Texas slope (LTS), Mississippi Canyon (MC), Mississippi–Alabama slope (MAS), and the Sigsbee Escarpment (SE). The NS profiles are perpendicular to the isobaths (represent the dip), and WE profiles are along isobaths (represent the strike) of the study area. Water depth is sampled every 0.5 km.

basins of 5–30 km in diameter cover the study area. The domes are frequent in the upper slope; toward the middle slope they increase in size and become salt massifs (Bryant and Liu, 2000). Bottom relief is enhanced by venting of gas and oil, which creates carbonate mounds of up to 30 m in height (Roberts et al., 1999).

Despite the extensive geological knowledge and data available, few studies have examined seafloor gradient statistics of the northern continental slope of the Gulf of Mexico. Bryant and Liu (2000) estimated the mean gradient of the LTS as ~1° but local gradients as steep as 40°. This large variability is caused by numerous knolls, basins, diapiric salt, salt withdrawal, sedimentation, and venting of gas and oil (Roberts et al., 1999). The SE with slopes of up to 20° also contributes to this variability (Bryant and Liu, 2000). Adams and Schlager (2000) examined two depth profiles across the continental slope in the eastern Gulf of Mexico to study subsurface curvature and its relationship to sedimentation processes. Roberts et al. (1999) reported gradients of up to 20° between water depths of 1,000 and 2,000 m in the eastern Gulf. Over the continental shelf, Resio et al. (1974) and Everts (1978) studied bottom profiles from Florida to Texas for coastal engineering applications, but these works were confined to water depths <100 m.

Oceanographically, the interaction of topography and flows gives rise to many interesting and new phenomena. Topographic boundaries reflect, refract, generate, and dissipate energy, e.g., LeBlond and Mysak (1978) and Gill (1982). The magnitude of the interactions depends on the physical characteristics of the seafloor, flow speeds, earth rotation, and stratification of the water column. Relief on the seafloor obstructs flows (Hogg, 1980) and induces bottom friction and large vertical rates of mixing across isopycnals (Polzin et al., 1997; Ledwell et al., 2000). These elevated mixing rates near high relief zones account for the mixing needed to close budgets of oceanic water overturns. Seafloor gradients, earth rotation, and

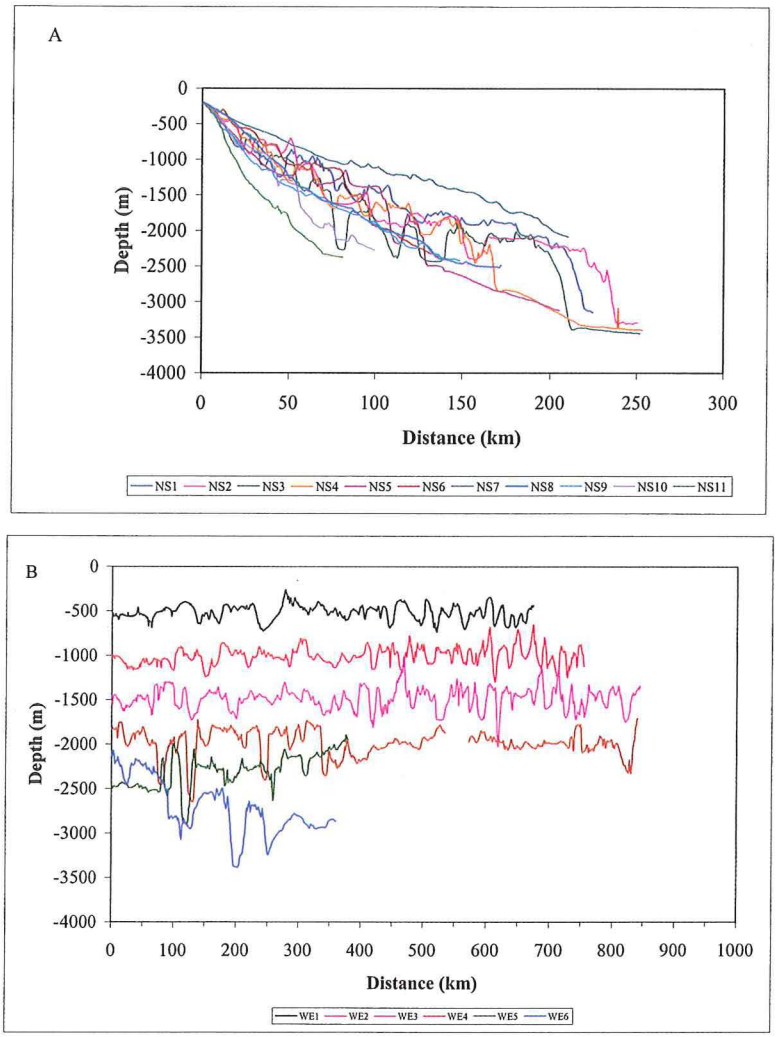

Fig. 2. Bathymetric profiles based on the (A) NS and (B) WE profiles. Note the overwhelming presence of the SE (panel A) with relief of ~1,000 m.

stratification affect TRW characteristics; studies relating directly to this study area include those of Hamilton (1990), Hamilton and Lugo-Fernández (2001), and Oey and Lee (2002). The present study attempts to examine seafloor gradients and roughness and discuss some implications of these bottom characteristics for the Gulf's ocean circulation.

Materials and Methods

The extent of the study area is 87.5–93°W over the northern continental slope (Fig. 1), in water depths of 200–3,400 m. This region was selected for several reasons. First, the National Oceanic and Atmospheric Administration completed a multibeam sonar survey of this region, providing the most current and accurate regional bathymetric data. Second, the region is important to the Minerals Management Service because of the high leasing and exploration activities by the oil and gas industry. Finally, several hydrographic and geological surveys, current measurements, and numerical modeling studies are underway or planned for this region; thus, our results can have direct bearing on these scientific endeavors.

To conduct our analyses, we extracted 11 cross-slope (NS) profiles and six along-slope (WE) profiles from our bathymetry database (Fig. 2) using ArcView software. The 11 NS profiles were distributed as follows: six over the LTS, one along the MC, and four over the

MAS. The WE profiles followed selected isobaths. The number of profiles analyzed in this study is high, especially when compared with five profiles that Amery (1978) used to describe and characterize the continental slope between Alabama and Texas.

The NS profiles, labeled from west to east, start near the shelf break or close to 200 m and end in water depths of 2,500–3,400 m. To study the seafloor gradient or dip, the NS profiles were set, as close as possible, perpendicular to smoothed isobaths. The requirement of orthogonal layout between profiles and isobaths resulted in lines that are unevenly spaced and not straight but represent the actual NS seafloor gradient. Length of the NS lines ranged from 80 to 250 km, depending on the location (Fig. 2A). Spacing of the NS profiles in the upper slope ranged from 30 to 80 km but was more variable in the lower slope. The WE profiles were set along the following isobaths: 500, 1,000, 1,500, 2,000, 2,500, and 3,000 m. These along-isobath profiles represent the strike and will yield information on roughness only. The length of WE profiles ranged from 400 to 1,000 km (Fig. 2B). Water depth along all profiles was sampled every 0.5 km, and each sample represents an average over a 200-m radius. Data gaps shorter than four points were filled using linear interpolation or the least-squared regressions, otherwise gaps were not filled.

All profiles were subjected to a battery of statistical and spectral analyses. Depth profiles were first plotted and inspected to detect problems and to ascertain shape and other general characteristics. Least-squared regression was applied to calculate the overall gradient of the NS profiles. Linear fits with r^2 values above 0.8 are deemed to describe accurately the profile; otherwise, a quadratic polynomial was fitted to the profile. The step-like SE was excluded from the fits. Adams and Schlager's (2000) analysis of depth profiles from around the world showed that over 80% of the profiles could be described by linear and power relationships.

Detrended water depth or residuals were used to estimate the root-mean-square (rms) bottom roughness (ε_{rms}) as (Fox and Hayes, 1985):

$$\varepsilon_{rms} = \sqrt{\frac{\sum_{i=1}^{n} (Z_i - \hat{Z}_i)^2}{n - 1}} \qquad (1)$$

In Equation 1, Z_i is the water depth, $\hat{Z}_i$ is the predicted water depth, and n is the number of observations. This estimator has the advantage of reducing the effects of long-wavelength gradients on the roughness estimate (Fox and Hayes, 1985).

Analysis of the profiles in the frequency domain requires preprocessing the bathymetric data plus considerations of the homogeneity or stationary assumption for these data (Fox and Hayes, 1985). The usual preprocessing consists of removal of the means and other trends from each profile. Next, the geological setting is examined with the objective of defining homogeneous areas. This step connects the known geology to the data analysis and is an important step. The SE was excluded again because this feature is nonstationary and cannot be analyzed by our techniques. Next, the profiles were divided into the LTS, MC, and MAS. The LTS profiles were further subdivided into upper and lower slope. The 1,500-m isobath is the divide between the upper and lower slope region following Amery (1978). The wave number (k) one-sided power spectrum [G(k)] was estimated from the residual water depths following the procedure of Bendat and Piersol (1986) using a Tukey–Cooley fast Fourier transform algorithm. A compromise between the profile length, the scale of interest (5–50 km), and the spectral estimate uncertainty [degrees of freedom (df)] resulted in subdividing the profiles into one to three segments of 128 points each. These parameters fixed the maximum scale at 64 km and the df at 2–6. The LTS spectra have 4–6 df, the MAS spectra have 2–4 df, and the MC's spectrum has 6 df. Water depth power spectra were fitted with a power law of the form $G(k) = ak^n$ following Bell (1975). A power law represents water depth spectra fairly consistently over many scales, and fractal geometry provides a theoretical basis for its applicability (Fox and Hayes, 1985). Bell (1975) found that, on average, $n = -2$, but one should expect variability around this value. The parameters of the power law also have simple physical interpretations (Bell, 1975; Fox and Hayes, 1985). Power spectrum also provides information about the bottom roughness and seafloor gradients. The gradient power spectrum $G_s(k)$ can be estimated directly from water depth spectrum as $4\pi^2k^2G(k)$ (Bendat and Piersol, 1986). A point of advice is that geologists use an amplitude spectrum instead of the power spectrum used here. Thus, the power law regression fits of the power spectra yield exponents whose values equal -2, and the "a" parameter is the square of that from the amplitude spectrum. For amplitude spectra the exponent is -1. Further, because of our definition of short-scale gradients, we have to

DOI: 10.18785/goms.2201.03

multiply by a 10^6 factor to compare the short gradient spectra with the water depth spectra.

Another analysis consisted of calculating the short-scale (1-km scale) gradients using centered finite differences. The resulting gradients were subjected to descriptive statistical characterizations and correlation analyses between profiles. The rms gradient for each profile is another measure of bottom roughness. Finally, the finite difference gradients power spectrum was computed following the procedures describe above, which yielded spectral estimates with ≤12 df. These were compared with the water depth spectra to investigate which relationship (power or exponential) best describes the gradient spectrum.

Results

Long-scale variations.—Cross-slope profiles: Figure 3 presents the 11 NS profiles grouped by shape similarity and physiographic province. All profiles start at a depth of about 200 m, and most have lengths of 150–260 km, except profiles NS10 and NS11, which have lengths of 100 and 80 km, respectively. All profiles reach depths of ~2,500 m. Profiles NS1–NS6 (Fig. 3A,B) cross the LTS at its widest part and the SE at its steepest section. The profiles NS1–NS3 (Fig. 3A) end just seaward of the escarpment, which shows as a step of ~1,000-m relief. The midsection of these profiles shows large depth variations, reflecting the large basins over the midslope (Bryant and Liu, 2000). Profiles 4–6 cross the escarpment near its eastern end as shown by their 1) diminished relief of the step toward the east; 2) occurrence of the step closer to the shelf break; 3) extension of ~150 km into the rise and abyssal plain; and 4) decrease of depth variations typical of midslope basins toward the east. The absence of the escarpment and basins reflects the high sediment input from the Mississippi River that covers these features (Amery, 1978). Profile NS7 (Fig. 3C) runs across the MC and is characterized by a monotonic depth increase and small depth variations across the profile. Profiles NS8–NS11 (Fig. 3C) represent the MAS and can be characterized as steep, with small depth variations, and a suggestion of leveling near their end. The latter reflects the Mississippi Fan where large sediment input and steep slopes induce mass movements and filling of the near rise and basin (Roberts et al., 1999). These conditions result in very steep upper gradients, e.g., shallower than 1,800 m, but leveling below as sediments accumulate.

Using the visual shape as guide, linear or quadratic functions were fitted to all profiles to determine the large-scale gradient. Table 1 shows the results of these calculations. All profiles except NS2 and NS3 are well described by a linear relation as indicated by high (>0.93) r^2 values. The gradients range from 0.00786 to 0.02776 (0.45–1.6°). These values agree with results of Bryant and Liu (2000), who found an average gradient of ~1° over the continental slope. The quadratic relations fitted to profiles NS2 and NS3 do an excellent job describing these profiles as indicated by r^2 values of 0.96 and 0.92, respectively. In curved profiles, the gradients are variable, and near the shelf edge, the gradients reach 0.02708 (1.6°), but near the end, the gradients are just about 0.003 (0.2°), as inferred from Figure 3C.

Figure 4 shows the power spectra in variance-preserving plots of the NS profiles without the SE, arranged from west to east or zonal, panels A through C. Most spectra are red, meaning that most energy lies at scales >64 km. Energy content is high in the western side of the study area (Fig. 4A); energy decreases toward the east (Fig. 4B) until reaching a minimum at the MC and increases again eastward of the MC (Fig. 4C). Note also the relatively insignificant energy levels at scales shorter than 7 km across the entire study area. Most spectra west of the MC display peaks between 13 and 21 km, and profiles NS2 and NS3 display a peak near 32 km. Spectra eastward of the MC suggest very small peaks at scales of 13–21 km. The energy minimum at MC and its vicinity reflects a smooth seafloor resulting from high influx and deposition of sediments from the Mississippi River and smaller rivers to the east. This high sediment input can cover and fill the intraslope basins. The energy increase westward of the MC reflects the sediment input reduction because of deposition. The intraslope basins have not been filled.

Because the LTS is subdivided into upper and lower slopes (Amery, 1978), the profiles NS1–NS5 were subdivided accordingly at the 1,500-m isobath into upper- and lower-slope profiles. Spectra were calculated for these subprofiles and pooled, following Bendat and Piersol (1986), to increase the df to 10. The pooled upper and lower spectra are shown in Figure 5. Again, the spectra are red, and energy is insignificant at scales shorter than 7 km. The upper-slope spectra contain more energy at longer scales, but the lower slope displays two prominent peaks at 32 and 16 km. The spectra suggest that the upper slope is smoother, but that the lower slope is more rugged,

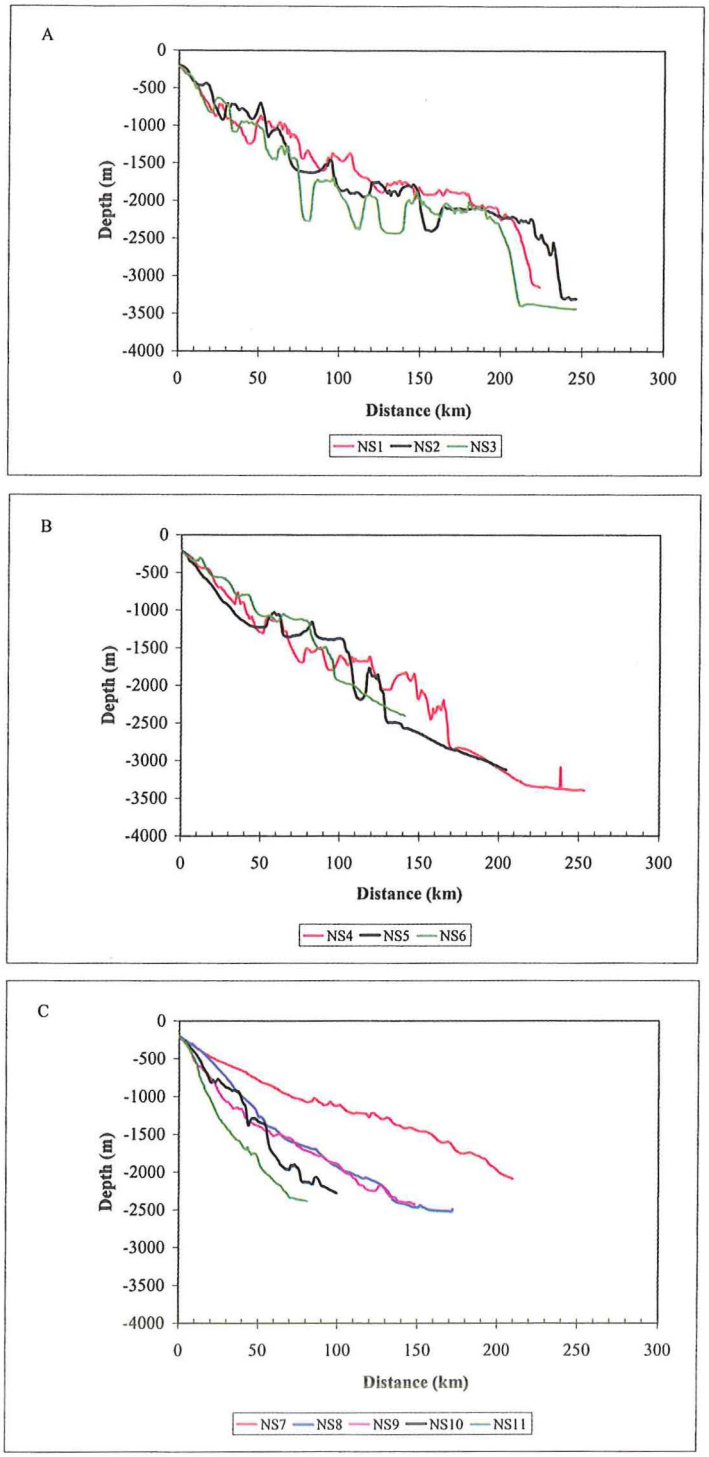

Fig. 3. The NS profiles sorted according to geometrical similarity from west to east. Note the gradual disappearance of the SE from west (panels A and B) to east (panel C).

DOI: 10.18785/goms.2201.03

TABLE 1. Least square parameters from linear and quadratic fits to water depth profiles.

Profile	Type	Gradient	Y-intercept (m)	a	r^2
NS1	Linear	0.00837	580.7	—	0.93
NS2	Quadratic	0.01989	177.1	0.0488	0.96
NS3	Quadratic	0.02708	124.6	0.0886	0.92
NS4	Linear	0.01318	354.9	—	0.96
NS5	Linear	0.01413	359.9	—	0.96
NS6	Linear	0.01621	152.4	—	0.98
NS7	Linear	0.00786	334.4	—	0.98
NS8	Linear	0.01460	404.4	—	0.96
NS9	Linear	0.01381	541.4	—	0.96
NS10	Linear	0.02244	242.8	—	0.97
NS11	Linear	0.02776	409.9	—	0.96

and that large intraslope basins are located in depths greater than 1,500 m.

In a previous work on water depth spectra, e.g., Bell (1975), water depth spectra are described by a power law with an exponent of −2. Figure 6 shows the power law exponents estimated for entire profiles and upper- and lower-slope NS profiles. Figure 6A shows the power law exponent from the entire profiles across the study area. The exponents vary from −1.8 to near −2.9, with a mean of −2.2. The 95% confidence interval of the mean shows that the mean is not statistically different from the theoretical value of −2. The distribution of the power law exponent shows a variation from west to east, with smaller values in the west and near −2 to the east. The power law exponent for the upper and lower slopes, plus those from NS6 to NS11 profiles, is shown in Figure 6B,C, respectively. Again, the mean value is not statistically different from −2, and its west to east variation decreases from the upper to lower slope. Note also that the exponents from the lower slope are very similar to those from the eastern study area. The r^2 values of these fits ranged from 0.88 to 0.97 for 10 profiles, and one had an r^2 value of 0.74, which means that the power law describes 74–97% of the variability of these spectra. This performance of the power law describing the water depth spectra is considered excellent.

Along-slope profiles: Because of the small latitudinal extent of the study area and data availability along the smoothed isobaths, only six WE profiles (WE1–WE6) were acquired from 500 m to about 3,000 m. These profiles cover the upper and lower LTS and the SE (Fig. 1) and are about two to four times longer than the NS profiles. Most profiles were ca. 420–850 km long (Fig. 2B). These profiles were sampled along smoothed isobaths and in most cases, varied little around the selected water depth and appear leveled. These profiles also represent the strike of the study area. The depth variations represent the intraslope basins. This was expected because the intraslope basins increase in size toward the midslope (Bryant and Liu, 2000). Exceptions are profiles WE5 and WE6, which show large deviations from the chosen water depth and reflect the SE presence. Examination of Figure 2B shows that the largest depth variations occur below 1,000 m, which agrees with results from the NS subprofiles. Because most profiles are leveled, the only preconditioning of these profiles consisted of removing the mean or demeaning.

The spectra for the demeaned profiles are shown in Figure 7. Because of the longer records, these spectra have double resolution as the NS spectra, and with longer records, the df were 10–12 except for the two short records. However, they resolve similar wave numbers as the NS spectra and are totally comparable. Although these WE spectra have insignificant energy at scales shorter than 7 km, like the NS spectra, at longer scales, they are fundamentally different. Instead of being red, they showed that energy is concentrated at scales of 21 and 64 km and very little energy between 13 and 20 km. In fact, some spectra, e.g., WE2, WE3, and WE5, show a significant peak right at 64 km. Comparison of the upper and lower panels on Figure 7 also suggests an energy increase toward the south. The shallower profiles (WE1 and WE2) are 10 times less energetic, WE3 is about two times less energetic, and WE4 and WE5 have similar energy as the NS profiles. However, the spectrum for WE6 is about two times more energetic than that for the NS profiles. Again, this energy increase toward the south reflects the presence of the intraslope basins at depths greater than 1,000 m and the presence of the SE.

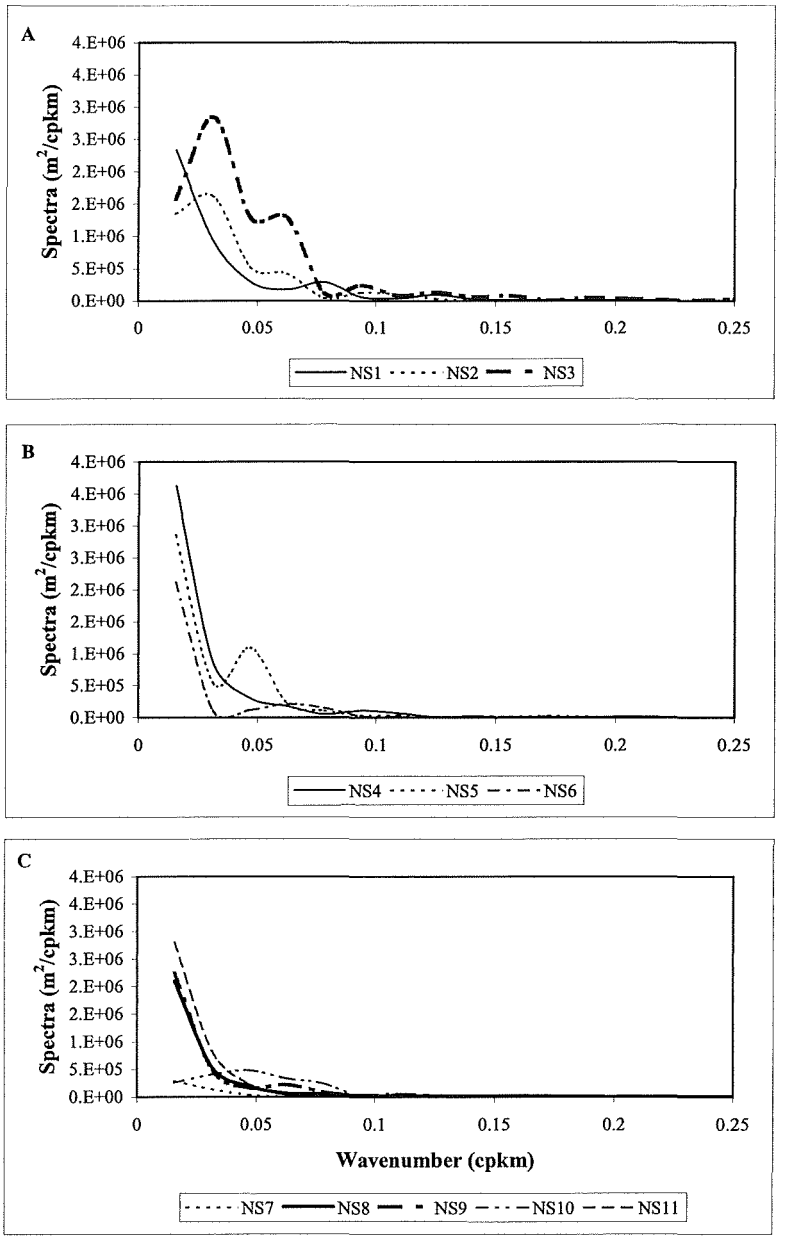

Fig. 4. Water depth power spectra of the NS profiles. These power spectra are red with peaks at 16 and 30 km. The df range from 2 to 6.

We explored how well the power law explains these spectra also. The results of the power law fitting are shown in Figure 6B. The exponents varied from −2.248 to −1.827. The average exponent is −2.060 with a SD of 0.147. These values are a bit smaller than those for the north–south profiles. The mean's 95% confidence interval (Fig. 6B) shows that the average exponent is different from −2. The r^2 values of 0.95–0.87 indicate that the power law does an excellent job describing these spectra for all except one where the r^2 value is only 0.72. The small but significant departure from k^{-2} dependence is probably the result of including the SE in the WE profiles, which is not a homogeneous feature, or because of a small sample.

Short-scale variations.—Cross-slope gradient profiles: The small sampling interval (0.5 km)

DOI: 10.18785/goms.2201.03

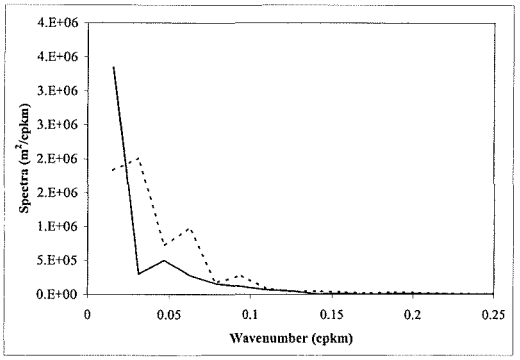

Fig. 5. Pooled water depth spectra from profiles NS1 to NS5 for the upper slope (US) and lower slope (LS). The boundary between upper and lower slopes is 1,500 m.

used allows examination of ~1-km-scale gradient variations. Figure 8A shows a typical short-scale gradient profile along line NS1. Short-scale gradients are very noisy, an expected result because numerical differentiation increases variability. These profiles exhibit a tendency for large gradient variations to be in "packets" of high values interposed with sections of small values and oscillate around negative values. The arithmetic average gradient of the 11 profiles, Table 2, ranged from −0.0088 to −0.0269 (0.5–1.5°). The average gradient is smallest at NS7 or the MC, near uniform to the west of the study area, and increasing slightly toward the east. The largest positive or upward gradients (8–16°) occur in the west side of the study area (NS1–NS5) and decrease to low values of 1.5–4° in the east (NS8–NS11). The large gradients to the west reflect the presence of the SE. The largest negative or downward gradients show a similar distribution as the positive gradients; they are high on the west (9–14°) and lower on the east (2–9°). The distribution of short-scale gradients (Fig. 9A) exhibits a low and broad normal or Gaussian shape, with most values occurring in the interval of −0.017 to 0.008 (0.5–1°), which agrees with a mean gradient of ~1° (Bryant and Liu, 2000). The distribution is slightly askew toward downward gradients, i.e., 53% of the values are negative, as expected. The maximum downward gradient is 0.252 (14°), whereas the maximum upward gradient is 0.287 (16°). This distribution of negative and positive gradients reflects the presence of many basins over the continental slope. Another statistic calculated from these profiles was the rms gradient, which is shown in Table 2. The rms gradients range from 0.0625 to 0.0213 (3.6–1.2°) and with similar west to east variation, steepest in the west and smallest in the east.

One can use the rms gradients to estimate an rms roughness height by using the definition of the gradient = $\Delta y/\Delta x$, where Δx (=1,000 m) is the distance between points used to evaluate the short-scale gradient. The roughness height estimated this way varies from 13 to 57 m. The roughness heights, computed using Equation 1, vary from 59 to 178 m, with most being over 129 m or near double the estimates from the rms gradients. The differences reflect the emphasis of scales or distance involved. The short scales reflect heights over 1 km, whereas the roughness derived from Equation 1 reflects the entire profile or hundreds of kilometers. Bell (1979) showed that, for 1-km scales, the roughness is tens of meters, but at scales equal to the profile lengths, the roughness should be about 100 m. Further, the "a" parameter of the depth power spectrum represents the squared amplitude of the 1-km component (Fox and Hayes, 1985). The height computed from the spectra ranges from 12 to 48 m. Because the rms height multiplied by $\sqrt{2}$ gives the amplitude of a sinusoid, the ratio of the rms height in Table 2 to the height derived from the spectra should equal $\sqrt{2}$ if both parameters are measuring the same. This ratio's mean value is 1.58, which is more than the expected value ($\sqrt{2}$ = 1.414). Further, the SD is 1.08, which is too large. The conclusion is that these two parameters are representing different aspects or factors. However, note the similarity of the roughness heights obtained from the spectra "a" parameters and those from the rms gradients.

Spectra of the short gradients are shown in Figure 10. Again, these spectra are red, have very low energy at scales shorter than 4 km, and show more peaks between 0.1 and 0.2 cpkm (5–10 km) than the water depth spectra. There is also a marked variation in energy from west to east. Energy is high in the first six profiles (NS1–NS6) and low in the remaining five profiles (NS7–NS11). Pooled spectra for the upper and lower LTS are shown in Figure 11. The lower slope has more energy than the upper slope, in agreement with the results from the water depth spectra. Further, both spectra are red with peaks at 16 and 21 km and little energy at scales shorter than 4 km. Plotting these spectra in a log–log format reveals near-constant values at wave numbers <0.2 cpkm (Fig. 12). These spectra are well represented by an exponential relationship, or $G_s(k) = B \exp(-mk)$. The exponential relationship accounts for between 80% and 93% of the

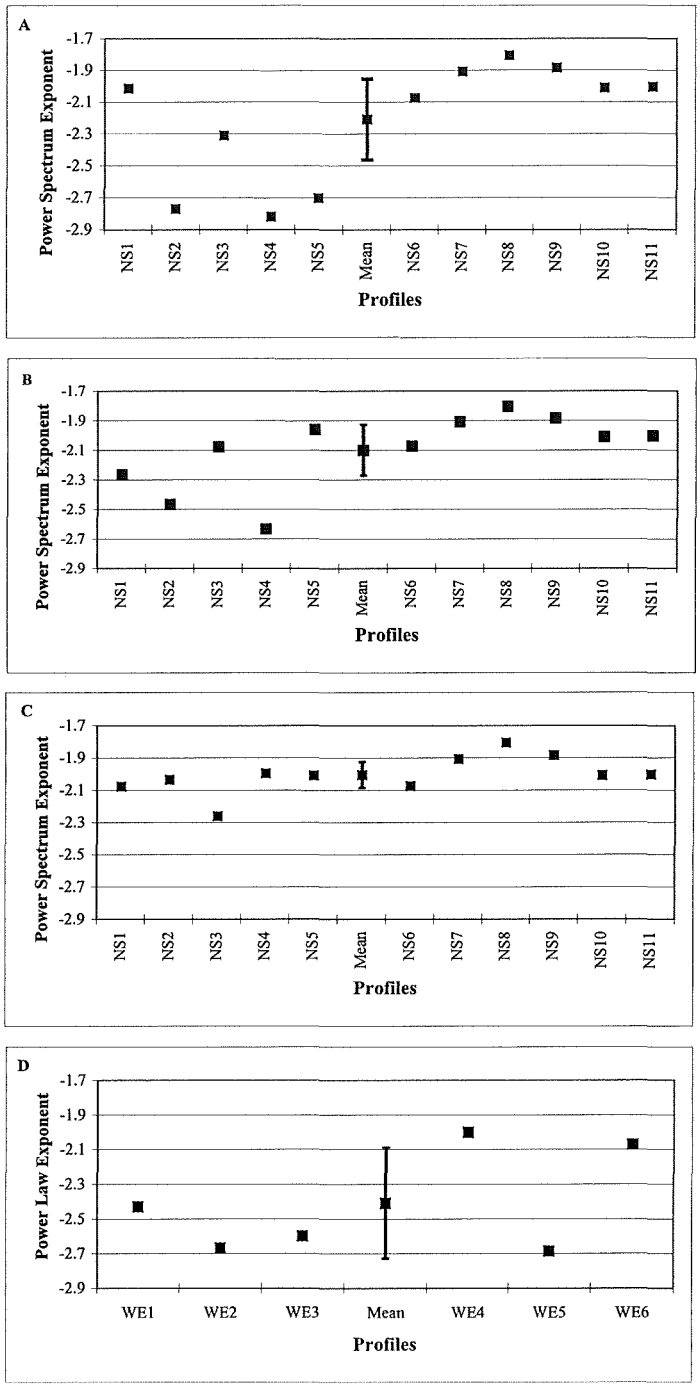

Fig. 6. Power law exponent (squares) estimated from the water depth power spectra of the (A) NS profiles, (B) upper-slope profiles, (C) lower-slope profiles, and (D) WE profiles. The average exponent (circle) with 95% confidence interval (bars). The mean values are not different from −2 except for panel D, where it is marginally different for −2.

DOI: 10.18785/goms.2201.03

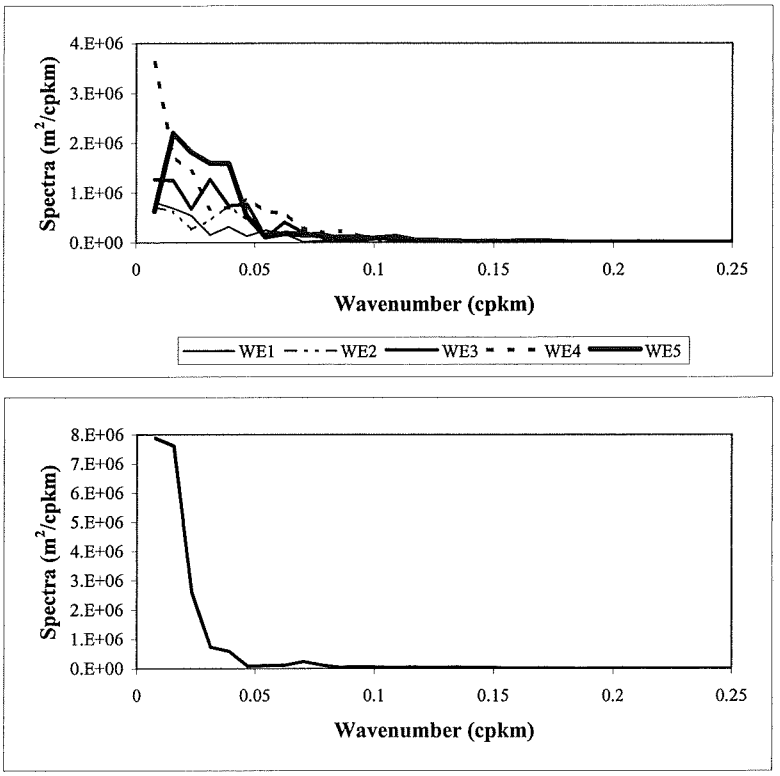

Fig. 7. Water depth power spectra of the WE profiles. These power spectra are red with peaks at 20 and 64 km. Note also the energy increase, e.g., scale change, from shallow (upper panel) to deep (lower panel) waters. The df range from 6 to 12.

spectrum variability (r^2 values of 0.80–0.93) for all except two cases (NS10 and NS11), where the exponential function accounts for 59% and 76% of the variability. The gradient spectrum and the water depth spectrum are related through the formula $G_s(k) = (2\pi k)^2 G(k)$ (Bendat and Piersol, 1986). Substituting the power law ($G(k) = ak^{-2}$) for the water depth spectra yields a constant gradient spectrum, given by $G_s(k) = 4\pi^2$ a, which is exactly what Figure 12 shows for wave numbers <0.2 cpkm. Similar results (not shown) were obtained for the pooled spectra of the upper and lower LTS. Figure 13A shows the constant from the gradient spectra and the value calculated from the depth spectra. Although there is variability, the mean values of 16,020 for the gradient spectra vs 10,114 estimated from the water depth spectra are statistically equal at the 95% confidence level.

Along-slope gradient profiles: Figure 8B shows a typical short-scale gradient profile (WE3) for the WE lines. Again, the profile is very noisy because of the numerical differentiation but reveals several similarities to the NS gradients. First, the magnitude of these gradients is similar, NS and WE gradient profiles have upward (positive) and downward (negative) gradients, and exhibits the "package" behavior observed for the NS gradients. An important difference is that these gradients oscillate very closely around zero, an expected result because these lines were sampled along isobaths. The arithmetic average gradient for these profiles (Table 2) ranges from −0.0003 to 0.0014 (−0.02° to 0.08°). The absolute values of the average gradient are nearly uniform in the upper or shallower profiles (WE1–WE4) and increase in the deeper lines (WE5 and WE6). Upward (positive) gradients have a maximum of 0.302 (17°) along WE4, and the remaining profiles have gradients of <14°. Downward (negative) gradients have a maximum of −0.214 (−12°), and the remaining lines have gradients of <10°. Note the similar range of downward and upward slopes, suggesting a symmetrical distribution. The distribution of the short-scale WE gradients (Fig. 9B) has a near-normal or Gaussian shape with a small spread or SD centered on 0.008. This distribution is more peaked than a normal distribution. As mentioned pre-

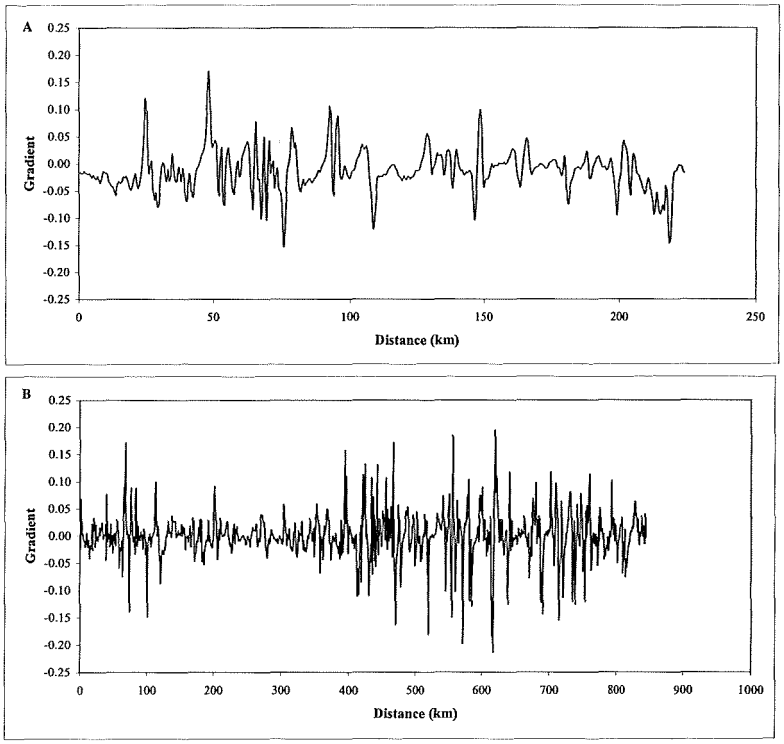

Fig. 8. Typical local gradient profiles along profile (A) NS1 and (B) WE3 computed using centered finite differences. Observed higher ruggedness for the WE and the apparent grouping of high values along profiles.

TABLE 2. Statistics of short-scale (1 km) gradients from water depth profiles.

Profile	Mean gradient	RMS gradient	Mean roughness (m)	ε_{rms} (m)
NS1	−0.0131	0.0406	40.6	141.9
NS2	−0.0123	0.0438	43.8	129.8
NS3	−0.0129	0.0574	57.4	178.1
NS4	−0.0126	0.0464	46.4	166.2
NS5	−0.0142	0.0405	40.5	176.4
NS6	−0.0155	0.0283	28.3	105.1
NS7	−0.0089	0.0133	13.3	58.7
NS8	−0.0134	0.0172	17.2	135.3
NS9	−0.0149	0.0213	21.3	116.5
NS10	−0.0208	0.0384	38.4	104.9
NS11	−0.0269	0.0334	33.4	131.6
WE1	0.0002	0.0223	22.3	84.0
WE2	−0.0003	0.0341	34.1	216.3
WE3	0.0002	0.0418	41.8	122.5
WE4	0.0002	0.0351	35.1	155.6
WE5	0.0014	0.0403	40.3	192.7
WE6	−0.0021	0.0319	31.9	306.9

viously, the variation between negative and positive gradients reflects the presence of large basins on this continental slope. Another statistic calculated from these profiles was the rms gradient (Table 2). The rms gradients range from 0.0223 to 0.0418 (1.3–2.4°) and are uniformly distributed from north to south. We used rms gradients to estimate a short-scale roughness height, as previously explained. The roughness height estimates (Table 2) ranged from about 22 to 41 m. The roughness heights estimated from Equation 1 for the WE profiles range from 84 to 307 m. The short-scale roughness and the rms heights are similar to the NS roughness.

Spectra of the 1-km gradients (Fig. 14) display many similarities to spectra of the NS gradients. First, there is very little energy at scale shorter than 4 km, these spectra are red, and there are many peaks at scales longer than 4 km, especially at scales of 10–32 km. There is an increase in energy toward the south. The relationship between the water depth and gradient spectra was examined, Figure 13B, and found to hold weakly at wave numbers <0.2 cpkm. The average spectrum value from the

DOI: 10.18785/goms.2201.03

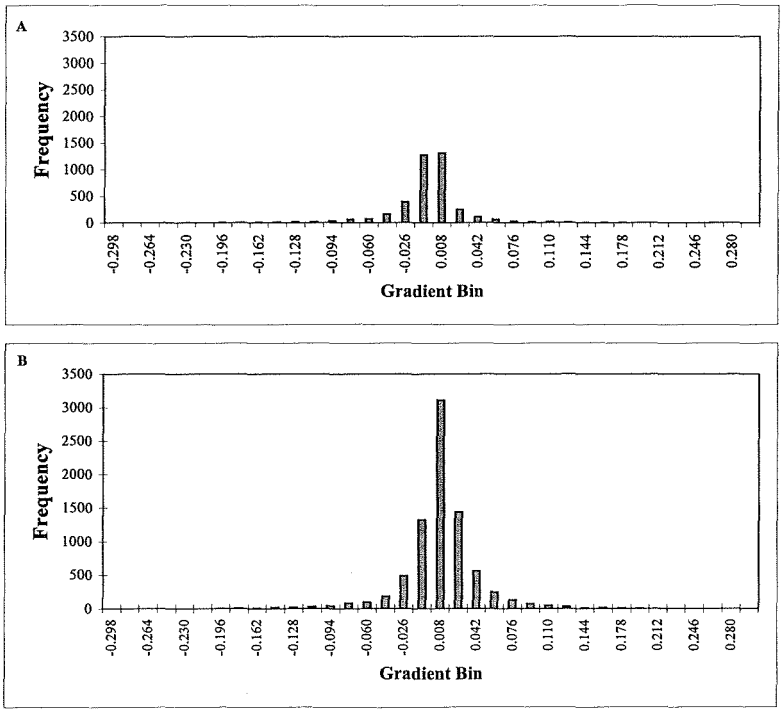

Fig. 9. Frequency histograms of the 1-km-scale gradients of the NS (panel A) and WE (panel B) profiles. Note two aspects of these histograms: first, they are slightly negatively skewed; and second, the NS histogram is flatter than a normal distribution but the WE histogram has a sharper peak.

water depth spectra is 8,404, and the value from the gradient spectra is 17,993, which statistically are barely equal at the 95% confidence level. Log–log plots of the gradient spectra reveal near-constant energy values at wave numbers <0.2 cpkm (Fig. 15), followed by a decreasing trend at higher wave numbers. These spectra are well represented by an exponential relationship, like their NS counterparts. The r^2 values of these fits are over 90%. Thus, the exponential relationship describes over 90% of the spectrum variability.

Oceanographic considerations.—Seafloor topography and gradients are very important for the generation and propagation of long waves (Rhines, 1970) and for dissipation of energy through bottom friction (Munk, 1997). Recently, it was found that bottom relief is very important and enhances vertical or diapycnal mixing (Polazin et al., 1997; Ledwell et al., 2000).

Stratification or stability of the water column plays important roles in the dynamics of deep-water circulation. In situ temperature (T) and salinity (S) over the study area (Nowlin et al., 2001) were used to estimate vertical profiles of seawater density. The in situ seawater density was estimated using the equation of state for seawater, 1980 (e.g., Pond and Pickard, 1983), and includes pressure effects. From these density profiles, the stability and Brunt–Vaisala frequency (N) were estimated. The density profiles showed that near-bottom waters are in stable equilibrium. Average N over the LTS at 1,000 m is 2.05×10^{-3} rad·sec^{-1} and decreases to 8.72×10^{-4} rad·sec^{-1} at depths of 1,500 m. Over the MAS, the average N is 2.28×10^{-3} rad·sec^{-1} at 1,000 m and decreases to 1.4×10^{-3} rad·sec^{-1} at 1,500 m. In deeper waters, there are not enough data to estimate N. Note the small increase from west to east and reduction with increasing depth. The shallower estimates are close to the value used by Hamilton (1990) of 10^{-3} rad·sec^{-1}, and the deep values agree with those used by Oey and Lee (2002).

Seafloor gradients (Table 1) or earth rotation (or both) provides the restoring force to sustain Rossby waves (Rhines, 1970). Bottom gradients induced a Coriolis-like force or topographic β-effect similar to the latitudinal variation of the Coriolis parameter or planetary β-effect. Therefore, it is important to determine whether the topographic or planetary β-effect dominates. For the topographic β-effects to dominate the planetary β-effect, the bottom

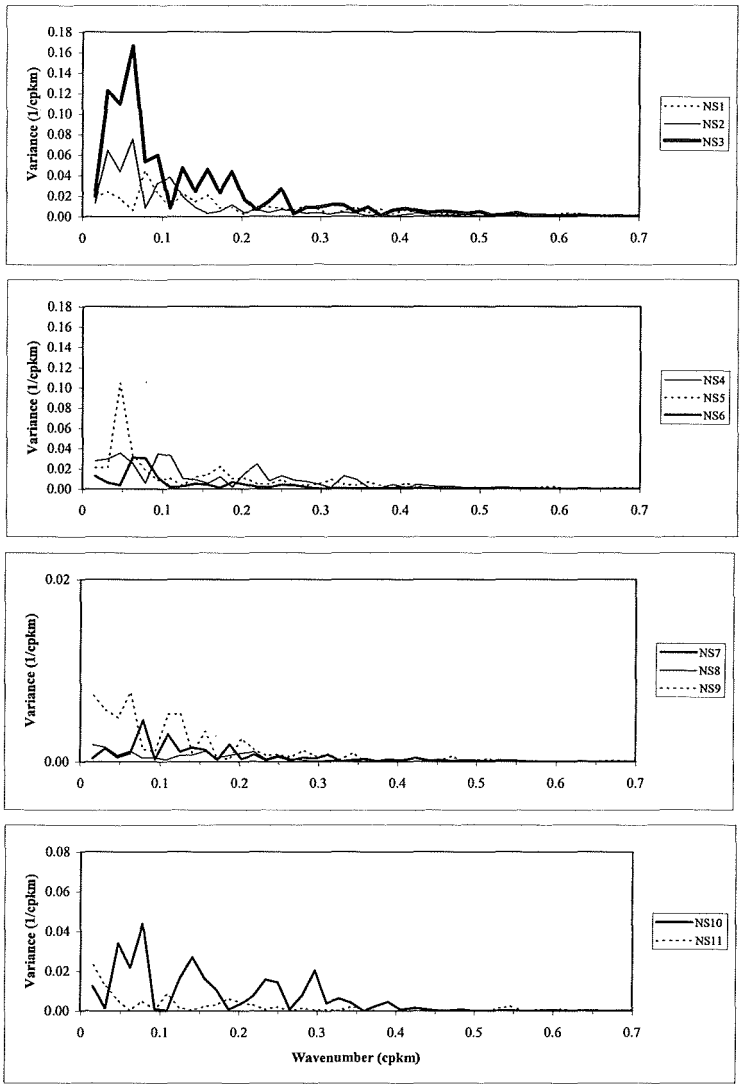

Fig. 10. Power spectra of the 1-km-scale gradients of the NS profiles. Most of these spectra are red with peaks at scales longer than 10 km. The df of these spectra ranged from 6 to 12. Note the scale change in the lower two panels.

gradient needs to satisfy the following relationship (LeBlond and Mysak, 1978):

$$\text{bottom gradient}(\alpha) > \frac{H}{a \tan \theta} \qquad (2)$$

where H is the water depth, a (=6,370 km) is the earth mean radius, and θ is latitude. Figure 1 shows that H ranges from 1,000 to 3,000 m, and that θ varies from 26° to 27.5°. Substituting these values, the right hand side of Equation 2 varies from 0.0003 to 0.00097. The north–south gradients range from 0.02 to 0.009 (Table 1), which are 10–100 times larger. Thus, topographic β-effects dominate in this region. Oey and Lee (2002) found similar results for this part of the Gulf.

Using a numerical model, Oey and Lee (2002) found a zone of high energy associated with TRWs along the SE. This band of high TRW energy coincides with steep gradients (16–20°) of the SE. Because topographic effects dominate over the planetary β-effect, the dispersion relation for TRWs on the LTS is:

$$\omega = \frac{-\alpha N \sin \phi}{\tanh\left(\frac{\text{NHK}}{f}\right)} \qquad (3)$$

where f is the Coriolis parameter (=2Ω sin θ),

DOI: 10.18785/goms.2201.03

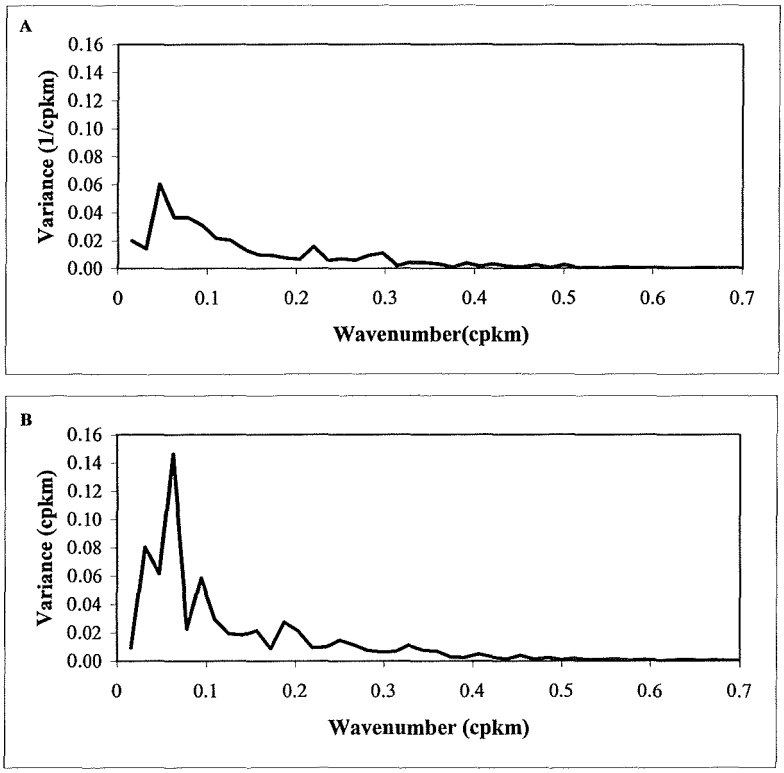

Fig. 11. Pooled spectra of the 1-km-scale gradients i profiles NS1–NS5 for the upper slope (US) and lower slope (LS). The boundary between upper and lower slopes is 1,500 m.

ϕ is the angle between K and the bottom gradient, K is the wave number vector for the TRWs, Ω ($=7.27 \times 10^{-5}$ rad·sec^{-1}) is the earth's angular velocity, and N is the Brunt–Vaisala frequency assumed constant. Equation 3 accepts two limits depending on the value of NHK/f. If NHK/f $\gg$1, then we have the short wave; if NHK/f $<$1, then we have the long-wave limit. From NHK/f, one can estimate a cutoff wavelength (λ_c) to decide which approximation to use. Substituting H = 3,000 m, N = 2.05×10^{-3} rad·sec^{-1}, and f = 6.6×10^{-5} rad·sec^{-1}, λ_c = 585 km. Hamilton (1990) and Hamilton and Lugo-Fernández (2001) estimated TRWs' wavelengths of 80–210 km, which are $<\lambda_c$; hence, over the LTS there are short TRWs. Because tanh(x) approaches 1, when x $\gg$ 1, then Equation 3 can be approximated as:

$$\omega = -\alpha N \sin \phi \qquad (4)$$

From Equation 4, the maximum TRW frequency in this region is given by $f_{max} = \alpha N$. Using mean gradients (Table 1), f_{max} ranges from 1.7×10^{-5} rad·sec^{-1} to 4.87×10^{-5} rad·sec^{-1} at 1,000 m and 4.1×10^{-6} rad·sec^{-1} to 3.17×10^{-5} rad·sec^{-1} at 1,500 m. Minimum TRW periods based on these results are ~1–4 d at 1,000 m and ~2–18 d at 1,500 m. For comparison, Hamilton (1990) and Hamilton and Lugo-Fernández (2001) reported TRW periods of ~10 and ~20 d, respectively. These TRWs can induce significant (40–50 cm·sec^{-1}) currents near the bottom. These differences most probably reflect the use of a mean gradient value instead of a local value.

However, a more interesting aspect is the potential generation of TRWs by flow-over topography. Charney and Flierl (1981) showed that TRWs generation by flow-over topography is most efficient if the bottom consists of many hills and valleys and if resonant conditions occur. The resonance condition is:

$$\frac{\bar{u}k^2}{\beta} = 1 \qquad (5)$$

where $\bar{u}$ is the mean current, k is the seafloor wave number, and $\beta = 2\Omega \cos \theta / a$. The bathymetric profile spectra show peaks at wavelengths of 16, 20, 31, and 64 km. Equation 5 was evaluated with the following values: k calculated from the wavelengths; mean currents of 0.02 and 0.08 msec^{-1} from data reported by Hamilton and Lugo-Fernández (2001) and

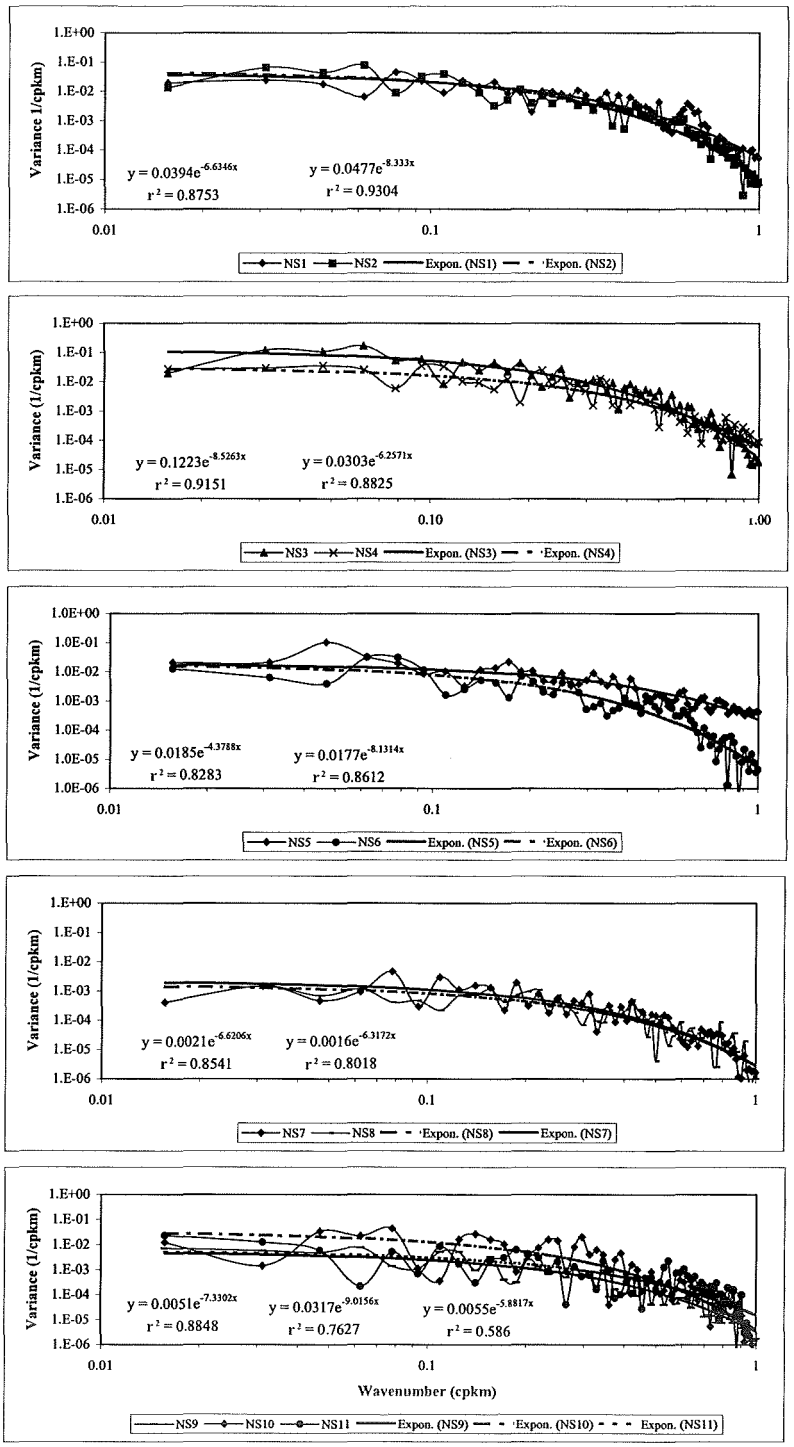

Fig. 12. Exponential regression fits to the NS profiles of the 1-km-scale gradient power spectra with r^2 values above 0.8 in general. Note the relatively constant energy at wave numbers <0.2 cpkm.

DOI: 10.18785/goms.2201.03

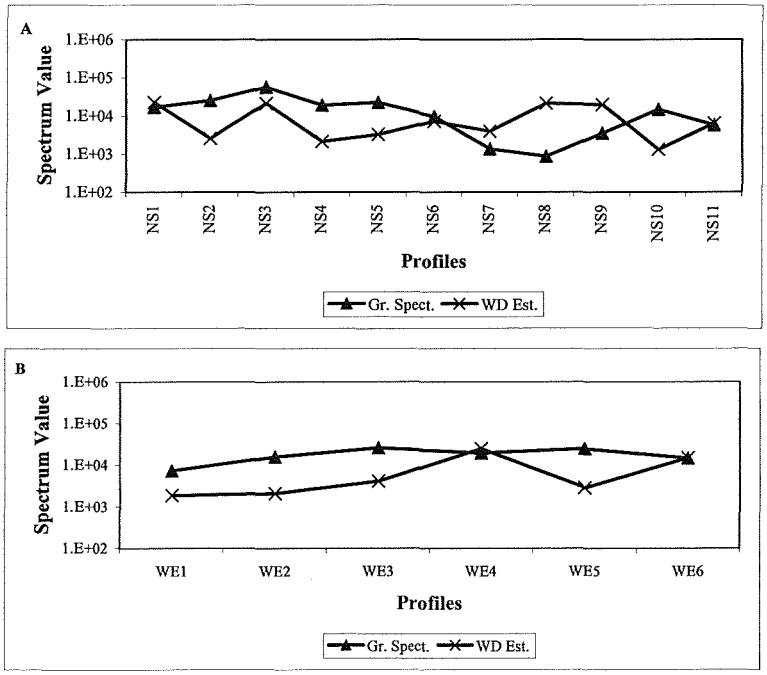

Fig. 13. Comparison of the constant power spectra of the gradients predicted from the water depth spectra with the spectra estimated from the gradient data. There are no statistical differences at the 95% confidence level between both estimates.

Nowlin et al. (2001); and $\beta = 2.03 \times 10^{-11}$ rad·min^{-1} sec^{-1}. The results show that the resonant condition is $\gg 1$ for all wavelengths, except at 64 km when the condition if O(1). Thus, we can rule out bottom-forced TRW generation at this site for short wavelengths but not at longer scales. One could ask what mean flows are needed to get resonant conditions in the LTS under the seafloor wavelengths found? The mean currents needed for resonance under these conditions are almost 0! However, Charney and Flierl (1981) state that these results need to be viewed with caution because of the limitations of their analysis. Stratification limits the effects of topography on flows to near the bottom. The vertical scale of topographic effects above the bottom is proportional to Lf/N, where L is the horizontal scale of the topography (Webb and Suginohara, 2001). Substituting the values above for L, N, and f, the vertical scale ranges from ~500 to 1,000 m. These vertical scales agree with those observed by Hamilton and Lugo-Fernández (2001). This criterion is similar to the vertical trapping coefficient (γ) given by NHK/f (Hogg, 2000). The trapping coefficient was evaluated for wavelengths of 80 and 200 km and water depths of 1,000–3,000 m. At 80 km, the trapping coefficient is relatively large and implies large trapping, especially as the water depth increases; for 200 km, the vertical trapping is small, which means hardly any bottom trapping. However, the vertical trapping observed in the Gulf (Hamilton, 1990; Hamilton and Lugo-Fernández, 2001) seems to be similar regardless of the differences in wavelengths observed.

Tide interaction with sloping bottoms is another area of concern, especially for generation of internal tides under stratified water columns. Internal tide generation depends on whether the bottom gradient is subcritical, critical, or supercritical (Holloway and Merrifield, 1999). This classification of the bottom gradient depends on whether α/s is smaller, equal to, or greater than 1, where s is defined as:

$$s = \pm\sqrt{\frac{\omega^2 - f^2}{N^2 - \omega^2}} \qquad (6)$$

where ω equals the frequency of the tide, and N and f retain their previous meanings. In the Gulf, the two dominant tides are the diurnal (K1 = 23.93 hr) and semidiurnal (M2 = 12.42 hr) (DiMarco and Reid, 1998). Evaluating Equation 6 using the previous values for N and f for both components yields s(K1) = 0.0151 and s(M2) = 0.0602. Comparing the mean gradients (Table 1) with s reveals that the LTS is

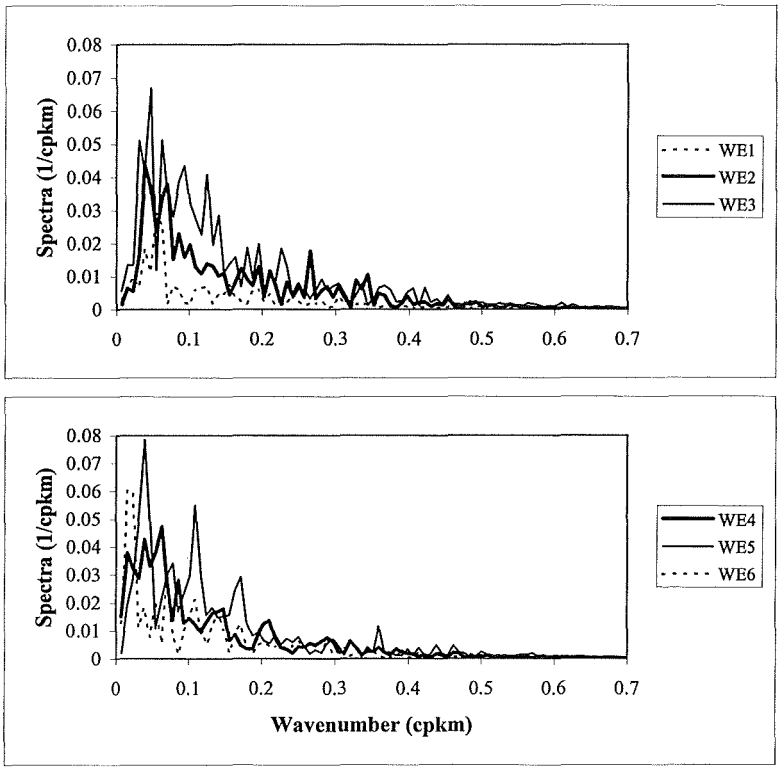

Fig. 14. Power spectra of the 1-km-sale gradients of the WE profiles. Most of these spectra are red with peaks at scales longer than 5 km. The df of these spectra ranged from 6 to 12.

critical and supercritical for diurnal tides and could be a source of internal tides. However, the semidiurnal tide is always subcritical, and internal tide generation is not expected. A similar result is found by calculating the critical frequency ($\omega_c = [(N \sin \alpha)^2 + (f \cos \alpha)^2]^{0.5}$), which for the LTS is 7.4×10^{-5} rad·sec^{-1} or a period of 24 hr. This means that diurnal tides are potentially very effective in causing mixing over the LTS. Ivey et al. (1995) indicated that significant mixing occurs over a frequency range ($0.8\omega_c \leq \omega \leq 1.8\omega_c$) instead of a narrow peak. Therefore, one would expect strong mixing for waves with periods of 13–33 hr, which includes the diurnal tide but excludes semidiurnal components. Waves of these periods (13–33 hr) induce high mixing over this rough topography, similarly to the high vertical mixing rates observed in the Brazilian basin (Polzin et al., 1997; Ledwell et al., 2000). The bottom roughness (Table 2) is high enough to make this region a very rough bottom, which should enhance mixing and energy dissipation.

Another relevant oceanographic aspect is the interaction of the ambient flow with fluids inside a basin. This is important because flows can help remove liquids from inside the basins. Baines (1995) indicated that fluid removal under stratified flows will occur if $2AN/\bar{u} \ll 1$, where 2A is the diameter of the valley, N and u retain their previous meanings. If $2AN/\bar{u} > 1$, fluids inside a basin will not be removed. At 1,000 m in the LTS, $\bar{u} = 0.3$ msec^{-1}, $N = 2.05 \times 10^{-3}$ rad·sec^{-1}, and 2A = 16–64 km; the criterion indicates that the fluids inside the basin are not removed. This occurs even if we used $N = 7.84 \times 10^{-4}$ rad·sec^{-1} and $\bar{u} = 1$ msec^{-1}. However, the fluid inside the basin will be sloping upward in the direction of the outer flow. Note that this criterion is independent of the basin depth. In the LTS, fluids inside the basins are generally hypersaline and thus denser than the overlaying water, which also prevents their removal from the basins.

Discussion

This study was undertaken to gain a better understanding of seafloor gradients on the northern continental slope of the Gulf of Mexico and possibly shed some light on the effects of these gradients on the observed circulation. We had hypothesized that eddies with diame-

DOI: 10.18785/goms.2201.03

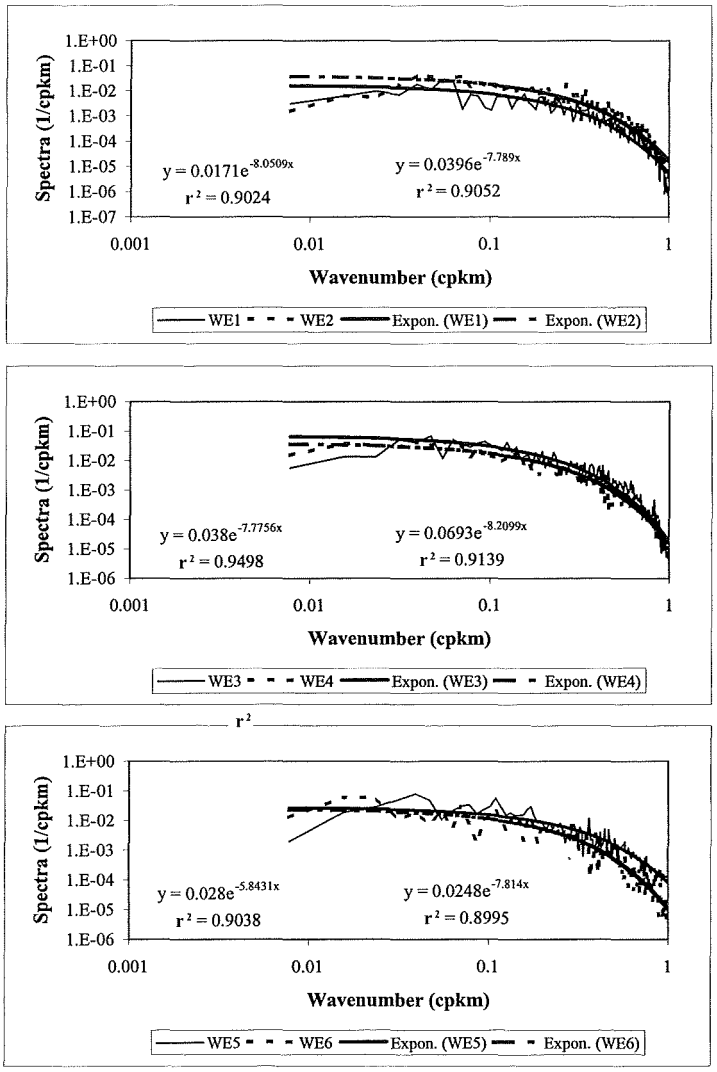

Fig. 15. Exponential regression fits to the WE profiles of the 1-km-scale gradient power spectra with r^2 values above 0.90. Note the relatively constant energy at wave numbers <0.2 cpkm.

ters of 40–150 km observed over this slope (Hamilton, 1992; Berger et al., 1996; Hamilton et al., 2002) were topographically generated. Testing these ideas required examination of the bottom profiles and their characteristics at long and short scales. We acquired 11 profiles perpendicular to the local isobaths and six profiles along the isobaths and sampled every 0.5 km. Water depths involved in the study area range from ~200 to over 3,000 m.

Most profiles or transects exhibit linear trends. The shape of the profiles or transects is related to the tectonics, underlying salt plates, and the sediment input. In the LTS area, sediment input and salt and plate tectonics influence the shape of the profiles, creating large diapirs that, when filled by sediment, create near-level seafloor. However, because sediment input increases the load, more diapirs are created, producing the basins observed on this area. Near the MC and MAS where present-day sediment input is still large because of proximity to the Mississippi River, the profiles are steep because of the sediment movement and accumulation near the foot of the slope, which covered the SE (Amery, 1978). The linear regressions account for over 80% of the profile variability and provided an estimate of the mean gradient over the entire profile. These average gradients are ~1° and agree with Bryant and Liu (2000). The SE influence on the profiles is manifested as a step feature

with a relief of ~1,000 m, except in the MAS, where high sediment input covered this feature. Short-scale gradients are highly variable, as expected, but their mean value is similar to that of the overall slopes, ~1°. However, individual gradients near the SE reach up to 16° in the LTS and decrease to 2–9° in the MAS area.

The 1-km-scale gradients suggest a very rough seafloor. Roughness heights (Table 2) for these 1-km gradients vary from 13 to 57 m. The rms roughness height is 58–307 m, or near six times as large. This height variation is caused by many intraslope basins, the dissolution of salt, and domes produced by gas and hydrocarbon expulsion over this area (Roberts et al., 1999; Bryant and Liu, 2000). Roughness heights derived from the water depth power spectra ranged from 12 to 48 m and are similar to the heights derived from the 1-km gradients. These roughness heights support the view of a very rough seafloor that should induce high bottom friction and energy dissipation.

Power spectra of all bathymetric profiles, Figures 4 and 7, are red, with most energy at scales longer than 10 km. The red nature of bathymetric spectra was reported by Bell (1975). The spectra, however, contain peaks near 16, 20, 31, and 64 km. We believe that these peaks represent the average diameters of the basins. Another possibility is that our profiles include a portion of the geologic transform fault field [average separation is 16 km, Stephens (2001)] present in this region. These spectra contain very little energy at scales shorter than 7 km, which fact agrees with the basin scale size of 5 km or larger (Roberts et al., 1999). As reported by Bell (1975) and Fox and Hayes (1985), these spectra can be described by a power law. The exponent (Fig. 6) resulting from using a power spectrum instead of an amplitude spectrum is −2, as expected. Although there is variability around this value, the 95% confidence interval indicates that the exponent is −2 except for the WE profiles. However, the WE profiles most probably do not represent a homogeneous sample because they include the SE. It is important to remember that the −2 value is justified by fractal geometry. We also tested the theoretical relationship between the water depth and the gradient power spectrum. We found that at wave numbers <0.2 cpkm, these two spectra are, on the average, related as required by theory (Figs. 12 and 15). This theoretical relationship implies that the gradient spectra are those of a white noise (white spectra have similar energy levels at all frequencies) or constant. The 1-km-scale gradients are numerical derivatives that have equal numbers of positive and negative values that resemble noise. This is especially true for scales longer than 4 km.

Oceanographically, the overall bottom gradients are large enough to make the topographic β-effect dominant over the planetary β-effect. However, because the seafloor slopes northward, the planetary and topographic β-effects reinforce each other (Rhines, 1970). Thus, we should expect anticyclones and associated cyclones commonly present in the study region to be strongly influenced by bottom slope. In addition, we should expect to see TRWs over this region, especially over the steep SE region.

Such TRW activity has been observed along steep slopes at other places, e.g., Hogg (2000) and Uehara and Miyake (2000). Hamilton and Lugo-Fernandez (2001) provided evidence for their existence along the SE. Oey and Lee (2002) discussed in detail how the local bathymetry and gradient affect the propagation, transmission, and reflection of TRWs in the study area. The height and spatial scales of the bottom roughness are large enough to affect the short-scale waves. For short-scale waves, the bottom feels very rough, but for the long-scale waves, the bottom feels smooth.

Bottom waters in this region are in a stable configuration as evidenced by the positive stability. Motions affected by buoyancy encompass frequencies of 8.7×10^{-4} rad·sec^{-1} to 2.3×10^{-3} rad·sec^{-1}, or periods of 0.8–2 hr. The TRWs' maximum frequencies estimated herein suggest periods of 2–18 d, which overlap the periods of 10–20 d reported by Hamilton (1990), Hamilton and Lugo-Fernández (2001), and Oey and Lee (2002) in this region. The analyses suggest that short TRWs should be bottom trapped but not the long ones; however, the available data show that short and long TRWs are trapped below 1,000 m. Rhines (1970) demonstrated that in a two-layer ocean, TRWs are confined mostly to the bottom layer. Because the Gulf of Mexico can be fairly well approximated as a two-layer ocean (Welsh and Inoue, 2000), thus TRWs should appear as bottom trapped. The analysis also revealed that TRW generation by flow over a wavy topography is unlikely in this region.

Because of the low zonal speeds observed and the scales at which the bottom profiles show energy, the cyclonic eddies with diameters of 40–150 km over the slope (Hamilton, 1992; Berger et al., 1996; Hamilton et al., 2002) cannot be ascribed to generation by flow

DOI: 10.18785/goms.2201.03

over a wavy topography as proposed by Charney and Flierl (1981).

Calculation of the critical frequency and slope reveals that this area can induce internal motions at frequencies of 13–33 hr. The frequency range includes diurnal periods and inertial motions at these latitudes but excludes semidiurnal components. One could expect high mixing induced by internal tides at diurnal periods or by inertial motions created by hurricanes (Hamilton et al., 2000). Finally, our analyses show that conditions over the study area are not conducive for removing fluids residing inside the basins. Basins, thus, could act as pockets for trapping gases, pollutants, or biological materials and possibly passive larvae. Geologically, these intraslope basins serve as sediment traps (Sinclair and Tomasso, 2002). These and other geological and biological implications of the basins need to be studied.

Conclusions

This study produced a detailed characterization of the seafloor over the northern slope of the Gulf of Mexico. Water depth profiles exhibit linear trends and mean bottom gradients of ~1° typical of the area (observed in nine of 11 cases). However, local bottom gradients of 16° occur along the SE. The analyses also reveal a very rough seafloor with roughness elements of 13–300 m, with most <100 m. Such rough bottoms could affect waves with wavelengths of tens of kilometers through bottom friction or diffuse reflection. Waves of hundreds of kilometers should be unaffected. This characterization includes the first estimation of water depth power spectra and of short-scale gradients in the Gulf of Mexico. Water depth spectra exhibit a k^{-2} dependence, whereas the 1-km gradient spectra are near constant at wave numbers <0.02 cpkm. Constant spectrum imply a white noise process. The spectra are red and reveal spatial scales of 10–64 km in the bathymetry findings, which agree with previous results. An important result is that NS transects in areas of near-zonal isobaths have directional derivatives very close to the actual bottom gradient. Oceanographically, the gradients are large enough to allow topographic β-effects to dominate over the planetary β-effect. This allows approximating the TRW dispersion in terms of the Brunt–Vaisala frequency and bottom gradients. The steep gradients of the SE can sustain periods of 2–18 d, which agrees with observed periods. Bottom trapping caused by stratification should be effective only for short waves, but observations suggest that bottom trapping is independent of wavelength. This discrepancy can be explained using the TRW theory in a two-layer ocean, where TRWs are essentially trapped in the bottom layer. The Gulf of Mexico can be approximated fairly well as a two-layer ocean, and TRWs are bottom trapped regardless of wavelength. Calculation of the critical frequency and slope shows that only diurnal and inertial frequencies (at this latitude) could be inducing strong vertical mixing in the study area, but this needs to be confirmed by experiments. The initial conjecture that cyclonic eddies with diameters of 40–150 km are generated by flow-topography interaction was not upheld because the resonance conditions are not met. Finally, the analysis reveals that little exchange occurs between fluids inside the basins with ambient slope waters.

Acknowledgments

The authors appreciate the support of the U.S. Department of the Interior, Minerals Management Service, Gulf of Mexico OCS Region, during the preparation of this manuscript. The opinions expressed by the authors are their own and do not necessarily reflect the opinion or policy of the U.S. Government. Comments from W. J. Wiseman, Jr. and an anonymous reviewer helped improved this work tremendously.

Literature Cited

Adams, E. W., and W. Schlager. 2000. Basic types of submarine slope curvature. J. Sediment. Res. 70: 814–828.

Amery, G. B. 1978. Structure of the continental slope, Northern Gulf of Mexico, p. 141–153. *In:* Framework, facies, and oil-trapping characteristics of the upper continental margin. Studies in geology, no. 7. A. H. Bouma, G. T. Moore, and J. M. Coleman (eds.). American Association of Petroleum Geologists, Tulsa, OK.

Baines, P. G. 1995. Topographic effects in stratified flows. Cambridge Univ. Press, Cambridge, United Kingdom.

Bell, T. H., Jr. 1975. Statistical features of sea-floor topography. Deep-Sea Res. 22:883–892.

———. 1979. Mesoscale sea floor roughness. Deep-Sea Res. 26:65–76.

Bendat, J. S., and A. G. Piersol. 1986. Random data analysis and measurement procedures. 2d ed. John Wiley & Sons, New York.

Berger, T. J., P. Hamilton, J. J. Singer, R. R. Leben, G. H. Born, and C. A. Fox. 1996. Louisiana/Texas Shelf Physical Oceanography Program: eddy circulation study, final synthesis report. Volume I: technical report. OCS Study MMS 96–0051. U.S. Department of the Interior, Minerals Management

Service, Gulf of Mexico OCS Region, New Orleans, 324 pp.

BRYANT, W. R., AND J. Y. LIU. 2000. Geology. *In:* Continental Shelf Associates, Inc. Deepwater Gulf of Mexico environmental and socioeconomic data search and literature synthesis. Volume 1: narrative report. OCS Study MMS 2000–049. U.S. Department of the Interior, Minerals Management Service, Gulf of Mexico OCS Region, New Orleans, 340 pp.

CHARNEY, J. G., AND G. R. FLIERL. 1981. Oceanic analogues of large-scale atmospheric motions, p. 504–548. *In:* Evolution of physical oceanography. B. A. Warren and C. Wunsch (eds.). MIT Press, Cambridge, MA.

DIMARCO, S. F., AND R. O. REID. 1998. Characterization of the principal tidal currents constituents on the Texas-Louisiana shelf. J. Geophys. Res. 103(C2):3093–3109.

EVERTS, C. H. 1978. Geometry of profiles across inner continental shelf of the Atlantic and Gulf coast of the United States. Technical report no. 78–4. U.S. Army Corps of Engineers, Fort Belvoir, VA. 92 pp.

FOX, C. G., AND D. E. HAYES. 1985. Quantitative methods for analyzing the roughness of the seafloor. Rev. Geophys. 23:1–48.

GILL, A. E. 1982. Atmosphere-ocean dynamics. Academic Press, New York.

HAMILTON, P. 1990. Deep currents in the Gulf of Mexico. J. Phys. Oceanogr. 20:1087–1104.

———. 1992. Lower continental slope cyclonic eddies in the central Gulf of Mexico. J. Geophys. Res. 97(C2):2185–2200.

———, T. J. BERGER, AND W. R. JOHNSON. 2002. On the structure and motion of cyclones in the northern Gulf of Mexico. J. Geophys. Res. 107(C12): 3208.

———, ———, J. J. SINGER, E. WADDELL, J. H. CHURCHILL, R. R. LEBEN, T. N. LEE, AND W. STURGES. 2000. Desoto Canyon eddy intrusion study, final report. Volume II: technical report. OCS Study MMS 2000–080. U.S. Department of the Interior, Minerals Management Service, Gulf of Mexico OCS Region, New Orleans, 275 pp.

———, AND A. LUGO-FERNÁNDEZ. 2001. Observation of high speed deep currents in the northern Gulf of Mexico. Geophys. Res. Lett. 28(14):2867–2870.

HOGG, N. G. 1980. Effects of bottom topography on ocean currents. GARP Publ. Ser. 25:167–205.

———. 1995. Some examples of topographic influences on the abyssal circulation, p. 137–139. *In:* Proceedings of the 'Aha Huliko'a Hawaiian Winter Workshop, University of Hawaii at Manoa, 17–20 Jan. 1995. P. Muller and D. Henderson (eds.). School of Ocean and Earth Science and Technology Special Publication, Honolulu, HI.

———. 2000. Low-frequency variability on the western flanks of the Grand Banks. J. Mar. Res. 58:523–545.

HOLLOWAY, P. E., AND M. A. MERRIFIELD. 1999. Internal tide generation by seamounts, ridges, and islands. J. Geophys. Res. 104(C11):25,937–25,951.

IVEY, G. N., P. DE SILVA, AND J. IMBERGER. 1995. Some examples of topographic influences on the abyssal circulation, p. 199–205. *In:* Proceedings of the 'Aha Huliko'a Hawaiian Winter Workshop, University of Hawaii at Manoa, 17–20 Jan. 1995. P. Muller and D. Henderson (eds.). School of Ocean and Earth Science and Technology Special Publication, Honolulu, HI.

KENNETT, J. P. 1982. Marine geology. Prentice-Hall, Englewood Cliffs, NJ.

LEBLOND, P. H., AND L. A. MYSAK. 1978. Waves in the ocean. Elsevier, Amsterdam.

LEDWELL, J. R., E. T. MONTGOMERY, K. L. POLZIN, L. C. ST. LAURENT, R. W. SCHMITT, AND J. M. TOLE. 2000. Evidence for enhanced mixing over rough topography in the abyssal ocean. Nature 403:179–182.

MUNK, W. 1997. Once again: once again-tidal friction. Prog. Oceanogr. 40:7–35.

NOWLIN, W. D., A. E. JOCHENS, R. O. REID, AND S. F. DIMARCO. 2001. Deepwater physical oceanography reanalysis and synthesis of historical data. Synthesis report. OCS Study MMS 2001–064. U.S. Department of the Interior, Minerals Management Service, Gulf of Mexico OCS Regional Office, New Orleans, 528 pp.

OEY, L.-Y., AND H.-C. LEE. 2002. Deep eddy energy and topographic Rossby waves in the Gulf of Mexico. J. Phys. Oceanogr. 32:3499–3527.

POLZIN, K. L., J. M. TOLE, J. R. LEDWELL, AND R. W. SCHMITT. 1997. Spatial variability of turbulent mixing in the abyssal ocean. Science 276:93–96.

POND, S., AND G. L. PICKARD. 1983. Introductory dynamical oceanography. 2d ed. Pergamon Press, New York.

RESIO, D., B. HAYDEN, R. DOLAN, AND L. VINCENT. 1974. Systematic variations in offshore bathymetry. Technical report no. 9, task no. NR389-158. Office of Naval Research, Arlington, VA. 28 pp.

RHINES, P. B. 1970. Edge-, bottom-, and Rossby waves in a rotating stratified fluid. Geophys. Fluid Dyn. 1:273–302.

———. 1977. The dynamics of unsteady currents, p. 189–318. *In:* The sea. Vol. 6. E. D. Goldberg, I. N. McCave, J. J. O'Brien, and J. H. Steele (eds.). John Wiley & Sons, New York.

ROBERTS, H. H., R. A. MCBRIDE, AND J. M. COLEMAN. 1999. Outer shelf and slope geology of the Gulf of Mexico: an overview, p. 93–112. *In:* The Gulf of Mexico large marine ecosystem. H. Kumpf, K. Steidinger, and K. Sherman (eds.). Blackwell Science, Malden, MA.

SINCLAIR, H. D., AND M. TOMASSO. 2002. Depositional evolution of confined turbidite basins. J. Sediment. Res. 72(4):451–456.

STEPHENS, B. P. 2001. Basement controls on hydrocarbon systems, depositional pathways, and exploration plays beyond the Sigsbee Escarpment in the Central Gulf of Mexico. *In:* Proceedings of the GCSSEPM Foundation 21st Annual Research Conference, Petroleum systems of deep-water basins; Gulf Coast Section of Economic Paleontologists and Mineralogists Foundation, Houston, TX.

SVERDRUP, H. U., M. W. JOHNSON, AND R. E. FLEMING.

DOI: 10.18785/goms.2201.03

1942. The Oceans. Prentice-Hall, Inc., Englewood Cliffs, NJ.

UEHARA, K., AND H. MIYAKE. 2000. Biweekly periodic deep flow variability on the slope inshore of the Kuril-Kamchatka Trench. J. Phys. Oceanogr. 30: 3249–3260.

WEBB, D. J., AND N. SUGINOHARA. 2001. The interior circulation of the ocean, p. 205–214. *In:* Ocean circulation and climate: observing and modeling the global ocean. G. Siedler, J. Church, and J. Gould (eds.). Academic Press, London.

WELSH, S. E., AND M. INOUE. 2000. LC rings and the deep circulation in the Gulf of Mexico. Geophys. Res. 105(C5):16,951–16,959.

OFFICE OF LEASING AND ENVIRONMENT (MS 5430), GULF OF MEXICO OCS REGION, 1201 ELMWOOD PARK BOULEVARD, NEW ORLEANS, LOUISIANA 70123-2394. Date accepted: March 5, 2004.